

Safe Heterogeneous Multi-Agent RL with Communication Regularization for Coordinated Target Acquisition*

Gabriele Calzolari * Vidya Sumathy *
 Christoforos Kanellakis * George Nikolakopoulos *

* Department of Computer Science, Electrical and Space Engineering,
 Luleå University of Technology, Luleå, Sweden.

Abstract: This paper introduces a decentralized multi-agent reinforcement learning framework enabling structurally heterogeneous teams of agents to jointly discover and acquire randomly located targets in environments characterized by partial observability, communication constraints, and dynamic interactions. Each agent's policy is trained with the Multi-Agent Proximal Policy Optimization algorithm and employs a Graph Attention Network encoder that integrates simulated range-sensing data with communication embeddings exchanged among neighboring agents, enabling context-aware decision-making from both local sensing and relational information. In particular, this work introduces a unified framework that integrates graph-based communication and trajectory-aware safety through safety filters. The architecture is supported by a structured reward formulation designed to encourage effective target discovery and acquisition, collision avoidance, and de-correlation between the agents' communication vectors by promoting informational orthogonality. The effectiveness of the proposed reward function is demonstrated through a comprehensive ablation study. Moreover, simulation results demonstrate safe, and stable task execution confirming the framework's effectiveness.

Keywords: Cooperative target acquisition, Safe autonomous coordination, Decentralized multi-agent reinforcement learning, Heterogeneous robotic systems, Learning-based control

1. INTRODUCTION

Heterogeneous multi-robot systems composed of Unmanned Aerial Vehicles (UAVs) and Unmanned Ground Vehicles (UGVs) offer complementary capabilities for complex missions such as surveillance, exploration, and search and rescue as highlighted by Shahar et al. (2025). UAVs provide wide-area perception and rapid mobility, while UGVs contribute endurance, payload capacity, and ground-level sensing. Coordinating such diverse platforms in complex and communication-constrained environments requires the autonomous agents to make decentralized decisions under partial observability and distinct motion dynamics. These challenges have motivated the growing use of distributed Multi-Agent Reinforcement Learning (MARL) to enable multi-robot cooperation in uncertain environments as analyzed by Wang et al. (2022). Recent advances have demonstrated the feasibility of learning decentralized control policies that scale to large teams and complex tasks as per Yu et al. (2022); Kuba et al. (2022); Jing et al. (2025). On-policy actor-critic methods such as the Multi-Agent Proximal Policy Optimization (MAPPO) algorithm have become strong baselines for cooperative tasks, while trust-region extensions, such as HAPPO and

HATRPO derived from Heterogeneous-Agent Trust Region Learning (HATRL) proposed by Zhong et al. (2024), improve training stability for heterogeneous agents. However, most of these frameworks ignore strong safety guarantees and inter-agent communication limitations, which restricts their deployment in physical robotic systems.

In parallel, graph-based neural architectures have emerged as an innate representation for relational reasoning and communication in multi-agent systems as presented by Niu et al. (2021); Hu et al. (2024); Liu et al. (2023). By modeling agents as nodes and their interactions as edges, such methods learn both who to communicate with and what to share. Despite their success, these approaches typically neglect the safety-critical aspects of real-world robotics. Recent advances in safe reinforcement learning have expanded both the theoretical and algorithmic foundations of constrained policy optimization and safe exploration Gu et al. (2024); Wachi et al. (2024). These works formalize diverse safety specifications, ranging from cost-based and probabilistic constraints to state-wise safety requirements, and analyze their implications for policy learning and constraint satisfaction. Even-then, integration with heterogeneous MARL and communication learning remains limited.

1.1 Related works

Multi-Agent Reinforcement Learning (MARL) has advanced cooperative control under uncertainty. In partic-

* This work was partially supported by the Wallenberg AI, Autonomous Systems and Software Program (WASP) funded by the Knut and Alice Wallenberg Foundation. The authors are within the Robotics and AI Group, Department of Computer Science, Electrical and Space Engineering, Luleå University of Technology, Sweden. Corresponding author's e-mail: gabcal@ltu.se

ular, the MAPPO framework investigated by Yu et al. (2022) shows that a simple actor-critic structure can yield robust policies with Centralized Training and Decentralized Execution (CTDE). Scalable MARL approaches aim to maintain learning efficiency and coordination as the number of agents grows. The work in Cui et al. (2025) presents an MADDPG-based UAV-USV collaborative decision-making method that enhances visual relative-position estimation via CNNs, introduces tailored multi-constraint reward functions for heterogeneous cooperation, and achieves faster convergence and superior performance compared to traditional strategies. In this context, Zhang et al. (2024) introduces a scalable constrained policy optimization framework called Scalable MAPPO-Lagrangian (Scal-MAPPO-L), that enables safe and decentralized learning in large multi-agent systems by employing local κ -hop policy updates, and thereby mitigating the exponential growth of the joint state-action space while preserving cooperative performance. The work in Okawa et al. (2023) introduces Information-sharing Constrained Policy Optimization (IsCPO), a MARL framework that sequentially updates agents' policies with shared surrogate-cost and divergence information to guarantee constraint satisfaction during learning and achieve sub-optimal yet safe multi-agent policies in large-scale control tasks. Guo et al. (2024) further improves cooperative decision-making by using MAPPO-PIS, an intent-sharing-driven cooperative decision-making framework for Connected and Autonomous Vehicles (CAVs) that integrates Intention Generator Module (IGM) and the Safety Enhanced Module (SEM) correction to improve multi-agent policy learning, achieving superior safety, efficiency, and traffic performance in human-machine mixed merging scenarios. Although these frameworks are effective, many do not explicitly guarantee physical safety or enforce dynamic feasibility constraints. Our approach extends this foundation by incorporating safety filters for real-time, model-consistent safety within a MAPPO structure. Communication learning has emerged as a critical component of decentralized coordination. The Multi-Agent Graph-attention Communication (MAGIC) framework proposed by Niu et al. (2021) employs a graph-attention communication protocol by jointly learning a Scheduler that determines when agents communicate and whom they address through a differentiable, attention-based dynamic graph encoder, and a Message Processor that applies Graph Attention Networks (GATs) over these dynamic graphs, enabling fully end-to-end training of communication structure and content. The Deep Hierarchical Communication Graph (DHCG) analyzed by Liu et al. (2023) learns directed acyclic communication structures by optimizing graph topology end-to-end, enabling convergent and efficient information flow among agents. Hu et al. (2024) proposes CommFormer that reframes communication as a graph learning problem using transformer-based attention to infer sparse and adaptive communication topologies. Similarly, Agent Transformer Memory (ATM) Yang et al. (2022) addresses partial observability in multi-agent RL by using a transformer-based working-memory mechanism to integrate factored entity observations with temporal information and to encode entity-specific action semantics. Sun et al. (2025) formalized communication redundancy through a dimensional analysis of message embeddings and

demonstrated that enforcing decorrelation within inter-agent representations significantly improves communication efficiency and cooperative performance in large-scale MARL systems. Comprehensive surveys Gronauer and Diepold (2022); Huh and Mohapatra (2024) emphasize the importance of adaptive, efficient communication. Our framework introduces a communication dissimilarity regularization term in the reward function that explicitly penalizes correlated message vectors.

The work in Fan et al. (2024) introduce an offline-compatible safe experience reshaping mechanism that learns underlying constraint geometry, projects unsafe actions onto its tangent safe space, and trains policies exclusively on these safety-corrected experiences. A pixel-observation safe RL algorithm that jointly learns a low-dimensional latent dynamics model and a latent barrier-like safety function to encode state-wise constraints with unknown hazard regions, enabling simultaneous safe policy optimization that significantly reduces safety violations and accelerates safety convergence while maintaining competitive reward performance is proposed in Zhan et al. (2024). To address the lack of a unified, practical methodology in SafeRL, where agents must optimize performance while minimizing risks of unintended harm, Ji et al. (2024) introduce a foundational, safety-centric framework that consolidates diverse RL algorithms into a cohesive, efficient research platform designed to streamline and accelerate progress in AI safety. Safe MARL frameworks Garg et al. (2024) and constrained optimization approaches Zhang et al. (2024) have begun exploring similar directions, but most remain centralized or homogeneous. Our work bridges this gap by embedding trajectory-aware safety filter for both holonomic (UAV) and differential-drive (UGV) agents directly into the decentralized MARL loop.

1.2 Our contribution

To address these challenges, this paper proposes a decentralized MARL framework for structurally heterogeneous agents, such as UAV-UGV teams, that combines graph-based communication, safety filters that evaluate the feasibility of the trajectory induced by each proposed action and rescale it in the event of a predicted collision, and stable on-policy learning. Moreover, a communication orthogonality regularization enforces representational dissimilarity among agents' message embeddings, mitigating interference and redundancy in shared communication channels. In particular, the main contributions are:

- A decentralized MARL architecture enabling coordination between structurally heterogeneous agents for collaborative target acquisition along with a communication orthogonality regularizer that promotes diverse messaging and robust multi-agent coordination.
- A trajectory-based safety filter that enforces collision avoidance by predicting the state evolution induced by each proposed action and rescaling unsafe actions when a future violation is detected, ensuring that the executed control inputs remain within the admissible safe set.
- Comprehensive ablation studies that quantify the contributions of goal-reaching, safety enforcement,

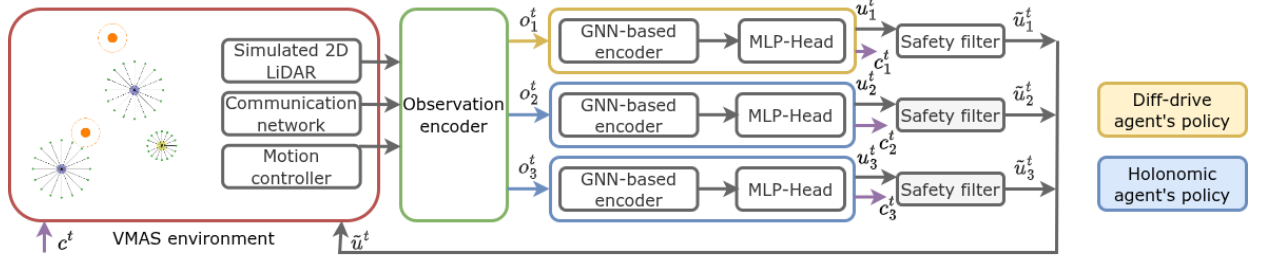


Fig. 1. Illustration of the VMAS environment in which three agents are trained to locate and acquire randomly placed targets (orange). The diagram highlights the key components of each agent's policy, including the GNN encoder, MLP heads, and safety filters.

and communication diversity to overall task performance.

2. METHODOLOGY

This section introduces the reinforcement learning framework in 2.1, the structure of the policy and critic networks in 2.2, the proposed safety filters in 2.3 and the reward function formulation in 2.4.

2.1 Reinforcement learning framework

The partially-observable environment consists of a continuous 2D squared workspace of side length d shown in Fig. 1 that includes n_t randomly distributed targets representing landmarks that n_h holonomic agents (UAVs) with radius r_h and n_d differential-drive agents (UGVs) with radius r_d have to explore and reach to. We denote by $\mathcal{H} = \{1, \dots, n_h\}$ and $\mathcal{D} = \{n_h + 1, \dots, n_h + n_d\}$ the sets of holonomic and differential-drive agents, respectively. The state of each agent i is

$$\mathbf{x}_i^t = \begin{cases} [\mathbf{p}_i^t, \mathbf{v}_i^t]^\top \in \mathbb{R}^4, & i \in \mathcal{H}, \\ [\mathbf{p}_i^t, \theta_i^t, v_i^t, \omega_i^t]^\top \in \mathbb{R}^5, & i \in \mathcal{D}, \end{cases} \quad (1)$$

where $\mathbf{p}_i^t = [x_i^t, y_i^t]^\top$ is the position, $\mathbf{v}_i^t = [v_{x,i}^t, v_{y,i}^t]^\top$ is the velocity (holonomic), θ_i^t is the heading, v_i^t the linear speed, and ω_i^t the angular speed of the agent i . Moreover, all agents are equipped with a simulated range sensor based on ray casting, which provides n_l range measurements indicating detected targets or the maximum sensing range, denoted r_h^l for holonomic agents and r_d^l for differential-drive agents. At the beginning of each episode, the agents have no prior information about the environment or target locations. A target $g \in \mathcal{G}$ is deemed considered covered when at least one agent lies within the distance threshold ρ_{cov} , as defined in Eq. (2).

$$\min_{i \in \mathcal{H} \cup \mathcal{D}} \|\mathbf{p}_i^t - \mathbf{p}_g^t\|_2 \leq \rho_{\text{cov}} \quad (2)$$

To explore the environment and find the targets, at each step t , each agent i outputs an action a_i^t composed by a continuous movement action $\mathbf{u}_i^t \in \mathbb{R}^2$ subject to the agent's dynamics and a communication vector $\mathbf{c}_i^t \in \mathbb{R}^{d_c}$. Agents are allowed to exchange information with agents within a finite communication radius r_c . These actions are computed by the policies based on some observations received from the environment at the beginning of the

step. In particular, each agent i receives an observation vector \mathbf{o}_i^t that combines its sensor measurements, the communication vector, and selected attributes of its own state as per Eq. (3).

$$\mathbf{o}_i^t = \begin{cases} (l_i^t, \mathbf{c}_i^t, \mathbf{v}_i^t), & i \in \mathcal{H}, \\ (l_i^t, \mathbf{c}_i^t, \mathbf{v}_i^t, \theta_i^t, \omega_i^t), & i \in \mathcal{D}, \end{cases} \quad (3)$$

where l_i^t denotes the range-sensor readings, \mathbf{c}_i^t the communication vector, \mathbf{v}_i^t the agent's velocity, θ_i^t the heading, and ω_i^t the angular velocity. Upon selecting an action \mathbf{u}_i^t , a safety filter Γ is applied, with its formulation defined in 2.3. The filter enforces safety constraints by projecting the nominal control input \mathbf{u}_i^t generated by the policy onto the admissible action set, resulting in the safe action $\tilde{\mathbf{u}}_i^t$. Thus ensuring that the executed command does not lead to collisions with other agents.

Holonomic agents are fully actuated in the plane and use a two-dimensional safe control input $\tilde{\mathbf{u}}_i^t = [\tilde{f}_x, \tilde{f}_y]^\top$, where each force component satisfies $\tilde{f}_x, \tilde{f}_y \in [-u_{\text{max}}, u_{\text{max}}]$. The safe control input directly affects the discrete-time dynamics, which can be written in state-update form as per Eq. (4).

$$\mathbf{x}_i^{t+1} = \begin{bmatrix} \mathbf{p}_i^{t+1} \\ \mathbf{v}_i^{t+1} \end{bmatrix} = \begin{bmatrix} \mathbf{p}_i^t + \mathbf{v}_i^t \Delta t \\ \mathbf{v}_i^t + \left(\frac{1}{m_i} \tilde{\mathbf{u}}_i^t - c_d \mathbf{v}_i^t \right) \Delta t \end{bmatrix} \quad (4)$$

where m denotes the agent's mass, Δt is the environment's time-step, and $c_d \geq 0$ represents the linear drag coefficient. Differential-drive agents evolve according to unicycle kinematics integrated via a fourth-order Runge-Kutta (RK4) scheme. Their safe control action is given by $\tilde{\mathbf{u}}_i^t = [\tilde{v}_i^t, \tilde{\omega}_i^t]^\top$, where the linear and angular velocities satisfy $\tilde{v}_i^t, \tilde{\omega}_i^t \in [-u_{\text{max}}, u_{\text{max}}]$.

2.2 Policy and critic networks

Each agent's policy is structured as a Graph Neural Network (GNN) encoder followed by a Multi-Layer Perceptron (MLP) output head. The first stage of each agent's policy is represented by a graph neural network (GNN) defined over a dynamic, position-dependent graph $\mathcal{G}_t = (\mathcal{V}, \mathcal{E}_t)$, where each node $v_i \in \mathcal{V}$ corresponds to an agent at time t . The edge set \mathcal{E}_t is constructed from the agents' spatial configuration, such that an edge exists between two agents if their Euclidean distance is within the predefined communication range r_c according to Eq. (5).

$$\mathcal{E}_t = \{(v_i, v_j) \mid \|\mathbf{p}_i^t - \mathbf{p}_j^t\|_2 \leq r_c, i \neq j\} \quad (5)$$

Each node feature vector contains the local observation of the corresponding agent. The GNN then constructs edge features by computing pairwise relational quantities, specifically the relative position $\mathbf{p}_i^t - \mathbf{p}_j^t$, the inter-agent distance $\|\mathbf{p}_i^t - \mathbf{p}_j^t\|_2$, and the relative velocity $\mathbf{v}_i^t - \mathbf{v}_j^t$. Message passing within the GNN is implemented using the GATv2Conv operator, proposed by Brody et al. (2022), which performs attention-weighted aggregation over neighboring nodes. After graph aggregation, each agent passes its embedding through a policy head conditioned on its dynamic model where each MLP consists of two hidden layers with 256 units and ELU activations followed by a linear output layer matching the action dimension. Furthermore, the critic is implemented using a DeepSets architecture proposed by Zaheer et al. (2018). The joint observation $\mathbf{o}^t = (\{\mathbf{o}_i^t\}_{i \in \mathcal{H}}, \{\mathbf{o}_i^t\}_{i \in \mathcal{D}})$ is first embedded through a local encoder $\phi(\mathbf{o}^t)$, and the global value is obtained by symmetric aggregation according to Eq. (6).

$$V(\mathbf{s}) = \rho \left(\frac{1}{N_a} \sum_{i=1}^{N_a} \phi(\mathbf{o}_i^t) \right), \quad (6)$$

where $\phi(\cdot)$ and $\rho(\cdot)$ are mappings realized as MLPs with ELU activations. In our setup, ϕ consists of two hidden layers of 128 neurons and ρ of two layers with 256 neurons.

2.3 Safety filters

To guarantee real-time safety, each agent's control input is projected onto the closest admissible control that satisfies a prescribed set of safety constraints, ensuring that the predicted trajectory remains collision-free. In particular, d_{safe} is the minimum required inter-agent separation to avoid collision.

Holonomic agents To guarantee collision avoidance under uncertain neighbor motion, it is proposed a safety filter that selects the closest feasible control input to the nominal force while ensuring that the agent's trajectory remains collision-free over the entire prediction horizon. For any candidate scaled control input $\tilde{\mathbf{u}}_i(\alpha) = \alpha \mathbf{u}_i^t$ where $\alpha \in \mathcal{A} = \{1.0, 0.8, 0.6, 0.4, 0.25, 0.1, 0.0\}$, the safety filter evaluates the feasibility of the resulting trajectory by propagating the agent's motion under $\tilde{\mathbf{u}}_i(\alpha)$ and verifying that it remains outside the maximum possible occupancy regions of all nearby agents. Among all feasible candidates, the control input corresponding to the largest admissible scaling factor is selected. In particular, the ego agent's trajectory is approximated over $\tau \in [0, \Delta t]$ as

$$\begin{aligned} \mathbf{p}_i^{t+\tau}(\alpha) &= \mathbf{p}_i^t + \left[\mathbf{v}_i^t + \frac{\Delta t}{2m_i} \mathbf{u}_i(\alpha) \right] \tau \\ \text{s.t. } & \|\mathbf{p}_i^{t+\tau}(\alpha) - \mathbf{p}_j^{t+\tau}\|_2 \geq d_{\text{safe}}. \end{aligned} \quad (7)$$

Each neighboring holonomic agent j possesses bounded per-axis velocities $\mathbf{v}_j^t \in [-v_{\text{max}}, v_{\text{max}}]$. This induces a worst-case reachable set at time $t + \Delta t$ described by the axis-aligned rectangle

$$\mathcal{R}_j^t = \{ \mathbf{p} \in \mathbb{R}^2 \mid \|\mathbf{p} - \mathbf{C}_j^t\|_\infty \leq \mathbf{H}_j \}, \quad (8)$$

where the center and half-size are given by

$$\mathbf{C}_j^t = \mathbf{p}_j^t + \frac{1}{2}(\mathbf{v}_{\text{min}} + \mathbf{v}_{\text{max}})\Delta t, \quad \mathbf{H}_j = \frac{1}{2}(\mathbf{v}_{\text{max}} - \mathbf{v}_{\text{min}})\Delta t. \quad (9)$$

To account for the circular bodies of the ego and neighbor agents, this set is inflated by the sum of agents' radii $r_i + r_j$ in the L_∞ metric,

$$\mathcal{R}_j^+ = \{ \mathbf{x} \in \mathbb{R}^2 \mid \|\mathbf{x} - \mathbf{C}_j^t\|_\infty \leq \mathbf{H}_j + (r_i + r_j + d_{\text{safe}}) \mathbf{1} \}. \quad (10)$$

In addition to holonomic neighbors, the environment contains differential-drive agents with maximum linear speed v_{max} . Over a short horizon Δt , the exact unicycle reachable set is a nonlinear subset of a circular sector whose angular width is bounded by $\omega_{\text{max}} \Delta t$. To enable efficient continuous-time collision checking, a conservative over-approximation is adopted by assigning to each diff-drive agent an isotropic velocity bound $\|\mathbf{p}_j^t\|_2 \leq v_{\text{max}}$ which implies that its position at time $t + \Delta t$ belongs to the disc

$$\mathcal{D}_j^t = \{ \mathbf{x} \in \mathbb{R}^2 \mid \|\mathbf{x} - \mathbf{p}_j^t\|_2 \leq v_{\text{max}} \Delta t \}. \quad (11)$$

This disc is inflated by the sum of agents' radii and an additional safety distance d_{safe} , yielding the conservative collision set

$$\mathcal{D}_j^+ = \{ \mathbf{x} \in \mathbb{R}^2 \mid \|\mathbf{x} - \mathbf{p}_j^t\|_2 \leq v_{\text{max}} \Delta t + (r_i + r_j + d_{\text{safe}}) \}. \quad (12)$$

Finally, it is selected the α that satisfies Eq. (13).

$$\begin{aligned} \max_{\alpha \in \mathcal{A}} & \quad \alpha \\ \text{s.t. } & \quad \mathbf{p}_i(t + \tau; \alpha) \notin \mathcal{C}, \quad \forall \tau \in [0, \Delta t]. \end{aligned} \quad (13)$$

where

$$\mathcal{C} = \left(\bigcup_{j \in \mathcal{H}} \mathcal{R}_j^+ \right) \cup \left(\bigcup_{j \in \mathcal{D}} \mathcal{D}_j^+ \right). \quad (14)$$

Differential drive agent Similar considerations are done for the definition of the safety filter used by the differential drive agent but in this case the forward evolution under $u(\alpha)$ is approximated using a fourth-order Runge–Kutta (RK4) integrator, and the interval $[0, \Delta t]$ is subdivided into 5 uniform substeps to produce intermediate states $\{x_k(\alpha)\}_{k=1}^5$. Each intermediate position $p_k(\alpha) \in \mathbb{R}^2$ is subjected to collision checks in a way analogous to the one discussed before for the holonomic agent.

2.4 Reward function formulation

At each step t , agent i receives a scalar reward r_i^t expressed by Eq. (15).

$$r_i^t = \mathbf{w}^\top \mathbf{r}_i^t = [w_{\text{dist}} \ w_{\text{goal}} \ w_{\text{coll}} \ w_{\text{comm}}] \begin{bmatrix} r_i^{\text{dist}}(t) \\ r_i^{\text{goal}}(t) \\ r_i^{\text{coll}}(t) \\ r_i^{\text{comm}}(t) \end{bmatrix}, \quad (15)$$

where $\mathbf{w} \in \mathbb{R}^4$ contains the reward weights and $\mathbf{r}_i^t \in \mathbb{R}^4$ the corresponding reward terms. These last terms capture progress toward targets, goal completion, collision avoidance, and communication diversity. The distance-based reward $r_i^{\text{dist}}(t)$ encourages agents to approach their nearest target and is defined as

$$r_i^{\text{dist}}(t) = \min_{g \in \mathcal{G}} \|\mathbf{p}_i^t - \mathbf{p}_g^t\| - \min_{g \in \mathcal{G}} \|\mathbf{p}_i^{t-1} - \mathbf{p}_g^{t-1}\|. \quad (16)$$

Moreover, when the agent covers a target, a fixed positive reward r_{goal} is assigned to $r_i^{\text{goal}}(t)$. To discourage

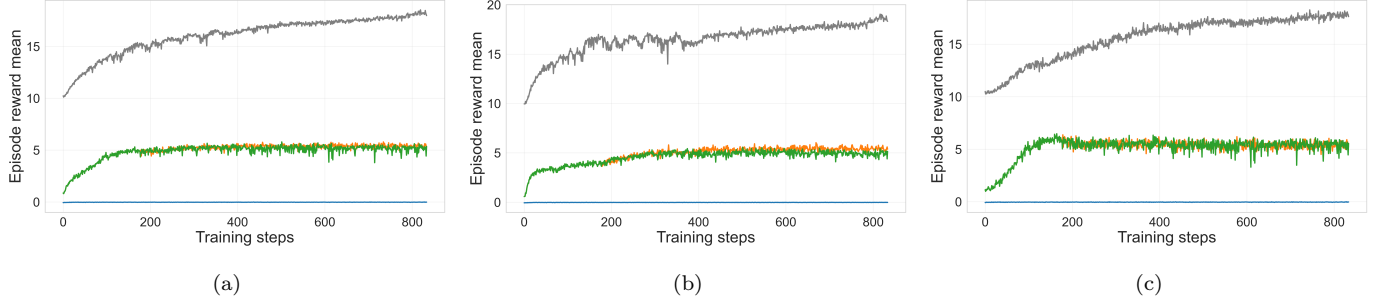


Fig. 2. Comparison of the mean episode reward trajectories for the full multi-agent system (a), holonomic agents (b), and diff-drive agents (c) under different reward shaping configurations. Reward schemes are color-coded as follows: R1 (blue), R2 (orange), R3 (green), and R4 (grey).

unsafe proximity to other agents, we define $r_i^{\text{coll}}(t) = r_{\text{coll}}$ whenever a collision happens. Furthermore, each agent produces a message vector $c_i^t \in \mathbb{R}^{d_c}$, and message diversity is encouraged via Eq. (17).

$$r_i^{\text{comm}}(t) = \sum_{j \neq i} (1 - \Gamma^2(c_i^t, c_j^t)), \quad \Gamma(c_i^t, c_j^t) = \frac{\langle c_i^t, c_j^t \rangle}{\|c_i^t\| \|c_j^t\|}, \quad (17)$$

To assess the contribution of the individual reward components, it is performed an ablation study using the progressively structured reward functions given by the reward terms vectors defined in Eq. 18. The analysis encompasses both the performance metrics recorded during policy training and the outcomes obtained in simulation over randomly generated environments, as reported in 3.2 and 3.3.

$$\begin{aligned} \mathbf{R1:} \quad & r_i^{(1)}(t) = [r_i^{\text{dist}}(t), 0, 0, 0]^\top, \\ \mathbf{R2:} \quad & r_i^{(2)}(t) = [r_i^{\text{dist}}(t), r_i^{\text{goal}}(t), 0, 0]^\top, \\ \mathbf{R3:} \quad & r_i^{(3)}(t) = [r_i^{\text{dist}}(t), r_i^{\text{goal}}(t), r_i^{\text{coll}}(t), 0]^\top, \\ \mathbf{R4:} \quad & r_i^{(4)}(t) = [r_i^{\text{dist}}(t), r_i^{\text{goal}}(t), r_i^{\text{coll}}(t), r_i^{\text{comm}}(t)]^\top. \end{aligned} \quad (18)$$

3. RESULTS

This section presents the training setup in 2.1 and the training and simulation results in 3.2 and 3.3, respectively.

3.1 Training

The agents are trained within a custom environment built on the VMAS simulator proposed by Bettini et al. (2022), configured according to the parameters reported in Table 1. Moreover, the training is performed using the BenchMARL framework proposed by Bettini et al. (2024), leveraging its implementation of the Multi-Agent Proximal Policy Optimization (MAPPO) algorithm. In particular, MAPPO is an on-policy actor-critic method adhering to the centralized training and decentralized execution (CTDE) paradigm, whereby each agent learns an individual policy, while a shared centralized critic is optimized using joint observations to stabilize multi-agent learning.

Table 1. Key environment and reward function parameters

Symbol	Value	Symbol	Value
n_d, n_h, n_t, d	1, 2, 3, 10m	w_{dist}	1.0
r_d, r_h, v_{max}	0.5m, 0.5m, 10m/s	w_{goal}	1.0
n_l, r_d^l, r_h^l	16, 1.5m, 3.0m	w_{coll}	1.0
$d_{\text{safe}}, \rho_{\text{cov}}$	0.05m, 1.5m	w_{comm}	0.1
$m, u_{\text{max}}, \Delta t, c_d$	1kg, 1, 0.1s, 0.25	r_{goal}	10.0
d_c, r_c	16, 4.5m	r_{coll}	-8.0

3.2 Training results

The agent policies have been trained for 834 optimization steps in 600 parallel environments using MAPPO. Figure 2a shows the evolution of the mean episode reward collected during training across the four reward configurations. Policies trained under R2 and R3 exhibit clear and stable convergence, following highly similar learning trajectories. In contrast, R1 remains close to zero throughout training, indicating that this reward configuration fails to provide a sufficiently informative learning signal. R4 achieves the highest episode rewards and shows evidence of convergence, although with noticeably higher variance. A similar behaviour is observed when analysing the mean episode reward per agent type, as shown in Figures 2b and 2c. For both R2 and R3, the differential-drive agent consistently achieves slightly higher rewards than the holonomic agents, whereas under R4 the holonomic agents marginally outperform the differential-drive one. The close correspondence between the per-agent reward curves across all reward configurations suggests that the learned policies support effective collaborative task execution, without inducing a pronounced asymmetric workload among the heterogeneous agents. Figure 3a reports the entropy evolution of the learned policies, which provides insight into the exploration-exploitation dynamics during training. Under R2, R3, and R4, entropy decays rapidly, indicating that the agents progressively acquire stable and consistent behaviours. Notably, for R2 and R3 the holonomic agents retain higher entropy for longer than the differential-drive agent, suggesting a degree of behavioural specialization. Conversely, R4 yields nearly identical entropy profiles across agent types, indicating more symmetric role emergence. In contrast, R1 maintains high entropy throughout training, reflecting persistent policy randomness and the absence of meaningful behavioural convergence.

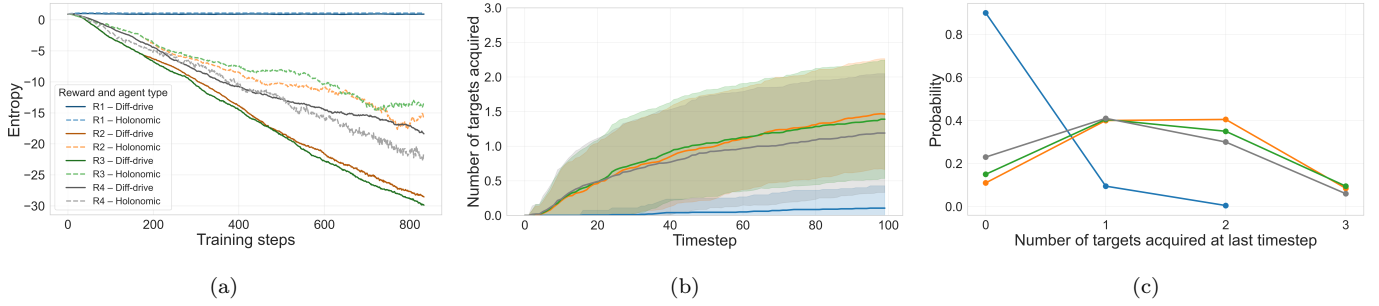


Fig. 3. (a) Entropy evolution for holonomic and diff-drive agents under the four reward configurations. (b) Mean number of acquired targets over time with standard deviation bands. (c) Probability mass function of the number of targets acquired at the final timestep. Colors denote reward schemes: R1 (blue), R2 (orange), R3 (green), and R4 (grey).

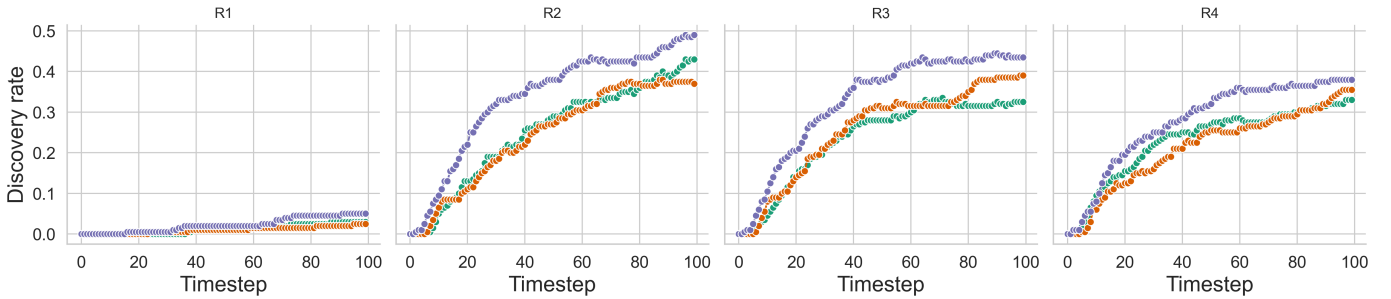


Fig. 4. Per-agent target discovery over time for the four reward configurations (R1–R4). Each subplot shows the mean discovery rate across simulations, with colored curves indicating the diff-drive agent (green), holonomic agent 1 (orange), and holonomic agent 2 (purple).

3.3 Simulation results

The trained policies have been further evaluated on 200 simulated environments, each executed for 100 timesteps, using scenarios consistent with those employed during training. Figure 3b reports the mean number of targets acquired over time and provides an overall indication of task execution efficiency. Policies trained with R1 exhibit minimal progress, confirming their inability to explore the environment effectively and to locate targets. In contrast, the policies trained with R2, R3, and R4 successfully acquire targets within the available time horizon. The steep initial increase observed for the latter configurations indicates that the agents have learned meaningful acquisition behaviours. However, the considerable variance associated with R2 and R3 suggests reduced robustness and a stronger dependence on the specific simulation instance. These observations are corroborated in Figure 3c, which shows the probability mass function of the number of targets acquired at the final timestep. Policies obtained with R2, R3, and R4 typically manage to acquire one or two targets, whereas R1 fails to achieve comparable performance in most evaluation runs. To assess the distribution of workload across the heterogeneous agents, Figure 4 presents the per-agent target discovery dynamics. R4 yields policies in which the discovery trajectories of the diff-drive and holonomic agents are closely aligned, indicating a more balanced workload and thus more symmetric collaboration. Conversely, R2 and R3 lead to more pronounced discrepancies between agents, revealing a degree of specialization and a less uniform allocation of the acquisition effort. Among these, R3 exhibits more stable behaviour than R2, as reflected by the lower variance in

entropy during training and by the clearer role differentiation observed for the two holonomic agents relative to the diff-drive agent. Across all evaluation metrics, policies trained under R1 demonstrate markedly inferior performance. They fail to develop reliable exploration or acquisition strategies and consistently underperform relative to the other reward configurations.

4. CONCLUSION

This work presents a decentralized multi-agent reinforcement learning framework for heterogeneous robotic teams for target acquisition in unknown environments, combining graph-based policies with safety filters to ensure collision-free coordination. The simulation results demonstrated stable learning, effective cooperation, and balanced workload distribution across agents under suitable reward shaping. Moreover, ablation studies confirmed the importance of goal-oriented, collision-avoidance, and communication-related reward terms. Future work will improve the performances in the target acquisition, investigate the efficacy of the framework with larger teams, and real-world deployment of the learned policies.

ACKNOWLEDGEMENTS

The computations were enabled by resources provided by the National Academic Infrastructure for Supercomputing in Sweden (NAIIS) and Chalmers e-Science Centre at C3SE, partially funded by the Swedish Research Council through grant agreement no. 2022-06725. Computations were performed on the Alvis cluster.

REFERENCES

Bettini, M., Kortvelesy, R., Blumenkamp, J., and Prorok, A. (2022). Vmas: A vectorized multi-agent simulator for collective robot learning. URL <https://arxiv.org/abs/2207.03530>.

Bettini, M., Prorok, A., and Moens, V. (2024). Benchmarl: Benchmarking multi-agent reinforcement learning. *Journal of Machine Learning Research*, 25(217), 1–10.

Brody, S., Alon, U., and Yahav, E. (2022). How attentive are graph attention networks? URL <https://arxiv.org/abs/2105.14491>.

Cui, Z., Guan, W., Qu, S., Hu, T., Hao, S., and Zhang, X. (2025). Uav-usv collaborative decision-making method based on multi-agent reinforcement learning. *IFAC-PapersOnLine*, 59(22), 639–644. 16th IFAC Conference on Control Applications in Marine Systems, Robotics and Vehicles CAMS 2025.

Fan, K., Chen, Z., Ferrigno, G., and Momi, E.D. (2024). Learn from safe experience: Safe reinforcement learning for task automation of surgical robot. *IEEE Transactions on Artificial Intelligence*, 5(7), 3374–3383.

Garg, K., Usevitch, J., Breeden, J., Black, M., Agrawal, D., Parwana, H., and Panagou, D. (2024). Advances in the theory of control barrier functions: Addressing practical challenges in safe control synthesis for autonomous and robotic systems. *Annual Reviews in Control*, 57, 100945.

Gronauer, S. and Diepold, K. (2022). Multi-agent deep reinforcement learning: a survey. *Artificial Intelligence Review*, 55(2), 895–943.

Gu, S., Yang, L., Du, Y., Chen, G., Walter, F., Wang, J., and Knoll, A. (2024). A review of safe reinforcement learning: Methods, theories, and applications. *IEEE Transactions on Pattern Analysis and Machine Intelligence*, 46(12), 11216–11235.

Guo, Y., Liu, J., Yu, R., Hang, P., and Sun, J. (2024). Mappo-pis: A multi-agent proximal policy optimization method with prior intent sharing for cavs' cooperative decision-making. In *European Conference on Computer Vision*, 244–263. Springer.

Hu, S., Shen, L., Zhang, Y., and Tao, D. (2024). Learning multi-agent communication from graph modeling perspective. URL <https://arxiv.org/abs/2405.08550>.

Huh, D. and Mohapatra, P. (2024). Multi-agent reinforcement learning: A comprehensive survey. URL <https://arxiv.org/abs/2312.10256>.

Ji, J., Zhou, J., Zhang, B., Dai, J., Pan, X., Sun, R., Huang, W., Geng, Y., Liu, M., and Yang, Y. (2024). Omnisafe: An infrastructure for accelerating safe reinforcement learning research. *Journal of Machine Learning Research*, 25(285), 1–6.

Jing, Y., Guo, B., Li, N., Xu, R., and Yu, Z. (2025). Federated multi-agent reinforcement learning: A comprehensive survey of methods, applications and challenges. *Expert Systems with Applications*, 293, 128729.

Kuba, J.G., Chen, R., Wen, M., Wen, Y., Sun, F., Wang, J., and Yang, Y. (2022). Trust region policy optimisation in multi-agent reinforcement learning. URL <https://arxiv.org/abs/2109.11251>.

Liu, Z., Wan, L., Sui, X., Chen, Z., Sun, K., and Lan, X. (2023). Deep hierarchical communication graph in multi-agent reinforcement learning. In E. Elkind (ed.), *Proceedings of the Thirty-Second International Joint Conference on Artificial Intelligence, IJCAI-23*, 208–216. International Joint Conferences on Artificial Intelligence Organization. Main Track.

Niu, Y., Paleja, R.R., and Gombolay, M.C. (2021). Multi-agent graph-attention communication and teaming. In *AAMAS*, volume 21, 20th.

Okawa, Y., Dan, H., Morita, N., and Ogawa, M. (2023). Multi-agent reinforcement learning with information-sharing constrained policy optimization for global cost environment. *IFAC-PapersOnLine*, 56(2), 1558–1565. 22nd IFAC World Congress.

Shahar, F.S., Sultan, M.T.H., Nowakowski, M., and Lukaszewicz, A. (2025). Ugv-uav integration advancements for coordinated missions: A review. *Journal of Intelligent & Robotic Systems*, 111(2), 69.

Sun, C., He, P., Wang, R., and Zheng, C. (2025). Revisiting communication efficiency in multi-agent reinforcement learning from the dimensional analysis perspective. URL <https://arxiv.org/abs/2501.02888>.

Wachi, A., Shen, X., and Sui, Y. (2024). A survey of constraint formulations in safe reinforcement learning. URL <https://arxiv.org/abs/2402.02025>.

Wang, Y., Damani, M., Wang, P., Cao, Y., and Sartoretti, G. (2022). Distributed reinforcement learning for robot teams: a review. *Current Robotics Reports*, 3(4), 239–257.

Yang, Y., Chen, G., Wang, W., Hao, X., Hao, J., and Heng, P.A. (2022). Transformer-based working memory for multiagent reinforcement learning with action parsing. In S. Koyejo, S. Mohamed, A. Agarwal, D. Belgrave, K. Cho, and A. Oh (eds.), *Advances in Neural Information Processing Systems*, volume 35, 34874–34886. Curran Associates, Inc.

Yu, C., Velu, A., Vinitsky, E., Gao, J., Wang, Y., Bayen, A., and Wu, Y. (2022). The surprising effectiveness of ppo in cooperative multi-agent games. In S. Koyejo, S. Mohamed, A. Agarwal, D. Belgrave, K. Cho, and A. Oh (eds.), *Advances in Neural Information Processing Systems*, volume 35, 24611–24624. Curran Associates, Inc.

Zaheer, M., Kottur, S., Ravanbakhsh, S., Poczos, B., Salakhutdinov, R., and Smola, A. (2018). Deep sets. URL <https://arxiv.org/abs/1703.06114>.

Zhan, S., Wang, Y., Wu, Q., Jiao, R., Huang, C., and Zhu, Q. (2024). State-wise safe reinforcement learning with pixel observations. In *6th Annual Learning for Dynamics & Control Conference*, 1187–1201. PMLR.

Zhang, L., Li, L., Wei, W., Song, H., Yang, Y., and Liang, J. (2024). Scalable constrained policy optimization for safe multi-agent reinforcement learning. In A. Globerson, L. Mackey, D. Belgrave, A. Fan, U. Paquet, J. Tomczak, and C. Zhang (eds.), *Advances in Neural Information Processing Systems*, volume 37, 138698–138730. Curran Associates, Inc. doi:10.52202/079017-4400.

Zhong, Y., Kuba, J.G., Feng, X., Hu, S., Ji, J., and Yang, Y. (2024). Heterogeneous-agent reinforcement learning. *Journal of Machine Learning Research*, 25(32), 1–67.